Effect of the protein ligand in DMSO reductase studied by computational methods

Dong, Geng; Ryde, Ulf

Published in:
Journal of Inorganic Biochemistry

DOI:
10.1016/j.jinorgbio.2017.03.004

2017

Document Version:
Early version, also known as pre-print

Effect of the protein ligand in DMSO reductase studied by computational methods

Geng Dong & Ulf Ryde *

Department of Theoretical Chemistry, Lund University, Chemical Centre, P. O. Box 124, SE-221 00 Lund, Sweden

Correspondence to Ulf Ryde, E-mail: Ulf.Ryde@teokem.lu.se, Tel: +46 – 46 2224502, Fax: +46 – 46 2228648

2018-05-01

Abstract
The DMSO reductase family is the largest and most diverse family of mononuclear molybdenum oxygen-atom-transfer proteins. Their active sites contain a Mo ion coordinated to two molybdopterin ligands, one oxo group in the oxidised state, and one additional, often protein-derived ligand. We have used density-functional theory to evaluate how the fourth ligand (serine, cysteine, selenocysteine, OH^-, O^{2-}, SH^-, or S^{2-}) affects the geometries, reaction mechanism, reaction energies, and reduction potentials of intermediates in the DMSO reductase reaction. Our results show that there are only small changes in the geometries of the reactant and product states, except from the elongation of the Mo–X bond as the ionic radius of X = O, S, Se increases. The five ligands with a single negative charge gave an identical two-step reaction mechanism, in which DMSO first binds to the reduced active site, after which the S–O bond is cleaved, concomitantly with the transfer of two electrons from Mo in a rate-determining second transition state. The five models gave similar activation energies of 69–85 kJ/mol, with SH^- giving the lowest barrier. In contrast, the O^{2-} and S^{2-} ligands gave much higher activation energies (212 and 168 kJ/mol) and differing mechanisms (a more symmetric intermediate for O^{2-} and a one-step reaction without any intermediate for S^{2-}). The high activation energies are caused by a less exothermic reaction energy, 13–25 kJ/mol, and by a more stable reactant state owing to the strong Mo–O^{2-} or Mo–S^{2-} bonds.

Keywords: DMSO reductase; Mo oxygen-atom-transfer proteins; density-functional theory; ligand variation; arsenate oxidase.

INTRODUCTION

Molybdenum (Mo) is a second-row transition metal that is involved in the metabolism of many biological molecules, e.g. in the biological cycles of carbon, nitrogen, and sulfur [1-3]. Enzymes employing Mo are present in almost all forms of life, including microorganisms, plants, and animals [1, 4]. Two groups of Mo enzymes have been found so far. One is the nitrogenases, which contain a complicated $MoFe_7S_9C$ cluster in the active site. The other is a large group of mononuclear Mo enzymes that catalyse mainly oxygen-atom-transfer (OAT) reactions between the Mo active site and various substrates. In this process, the Mo ion cycles between the +IV and +VI oxidation states. In all mononuclear Mo enzymes, one or two molecules of the special ligand molybdopterin (pyranopterin ene-1,2-dithiolate) bind bidentately to Mo.

The mononuclear Mo enzymes can be divided into three families, based on the structure of the active site, viz. the dimethyl sulfoxide reductase (DMSOR), the sulfite oxidase (SO), and the xanthine oxidase (XO) families [1, 5-7]. The active site of the enzymes in the DMSOR family contains two molybdopterin cofactors bound to the Mo ion in a nearly planar fashion [7, 8] and one deprotonated side-chain O, S or Se atom of serine, cysteine, or selenocysteine at the apical position. Some enzymes have a oxo or sulfido group instead of the protein-derived ligand [1, 7, 9]. In DMSOR, the reduced enzyme reacts with dimethyl sulfoxide (DMSO) to generate dimethyl sulfide (DMS) and the oxidised state of the enzyme, which contains one oxo group (Scheme 1) [1, 7]. The active site is then regenerated by two sequential steps of coupled electron and proton transfer. The reaction mechanism has been extensively studied by experimental methods [1, 10-15]. The studies have demonstrated that the reactivity strongly depends on the substrate [12] and that the rate-determining step involves the formation of the Mo–O bond and a two-electron transfer from the Mo(IV) centre to the substrate as the S–O bond breaks [15-17].

Scheme 1. The overall reaction of DMSOR

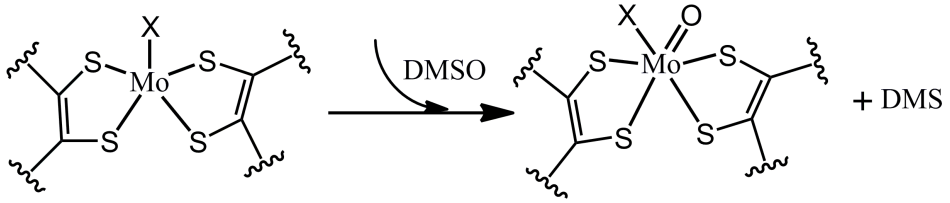

X=serine, cysteine, or selenocysteine

The DMSOR reaction mechanism has also been thoroughly studied with computational methods [16-27]. In 2001, Webster and Hall used the B3LYP method to show that the energy barrier of OAT is 37 kJ/mol, starting from the DMSO-bound intermediate [19]. A similar barrier was found by Mohr and coworkers [28]. Thapper et al. studied also the binding of DMSO and proposed a two-step mechanism, based on a slightly different model [20]. Subsequently, these findings were confirmed by several other groups [16, 17, 21, 22, 24, 29, 30]. The suggested reaction starts with DMSO binding to the Mo(IV) state of the active site to form an intermediate. In the second step, the S–O bond is cleaved in an OAT reaction [16, 23], which is coupled with a two-electron transfer from the Mo ion. All studies have indicated that the second reaction is the rate-determining step with a barrier of 38–80 kJ/mol [16, 19-24, 29, 30]. We have shown that the calculated barrier strongly depends on the theoretical method and that a proper account of dispersion and solvation effects is needed, together with large basis sets and accurate density functional theory (DFT) methods [17, 27]. All these mechanistic studies assumed that the protein-derived ligand was serine (modelled by CH_3O^-).

As mentioned above, three possible protein-derived ligands (serine, cysteine, or selenocysteine) may bind to Mo ion in the active site of members of the DMSOR family. McNaughton et al. performed a combined spectroscopic and DFT study of reduced models of DMSOR involving XCH_3^-, with X = O, S, or Se [31]. They studied the electronic structure, vibrational spectrum, and low-lying excited states. However, they did not study how the reaction mechanism and rate change when DMSO reacts with the enzyme with different protein-derived ligands. In this paper, we have studied the DMSOR reaction mechanism with alternative models of active site, varying the protein-derived ligand. This improves our understanding of DMSOR reaction mechanism and the effects of various ligands.

METHODS

In this paper, quantum-mechanical (QM) cluster calculations [32] were performed to study the reaction mechanism of DMSOR. Seven models were employed to investigate the effect of the protein-derived ligand (Figure 1). All models involve two molecules of dimethyldithiolene (DMDT, $CH_3SC{=}CSCH_3$), which is a common model of molybdopterin, both in experimental and computational studies [16, 17, 21, 22, 24, 29, 30]. CH_3O^-, CH_3S^-, and CH_3Se^- were used as models of serine, cysteine, and selenocysteine, respectively, whereas OH^-, O^{2-}, SH^-, and S^{2-} were tested as models of oxo and sulfido groups observed in some enzymes [1, 7, 9, 33]. The DMSO substrate was explicitly modelled and it was converted to DMS during the reaction.

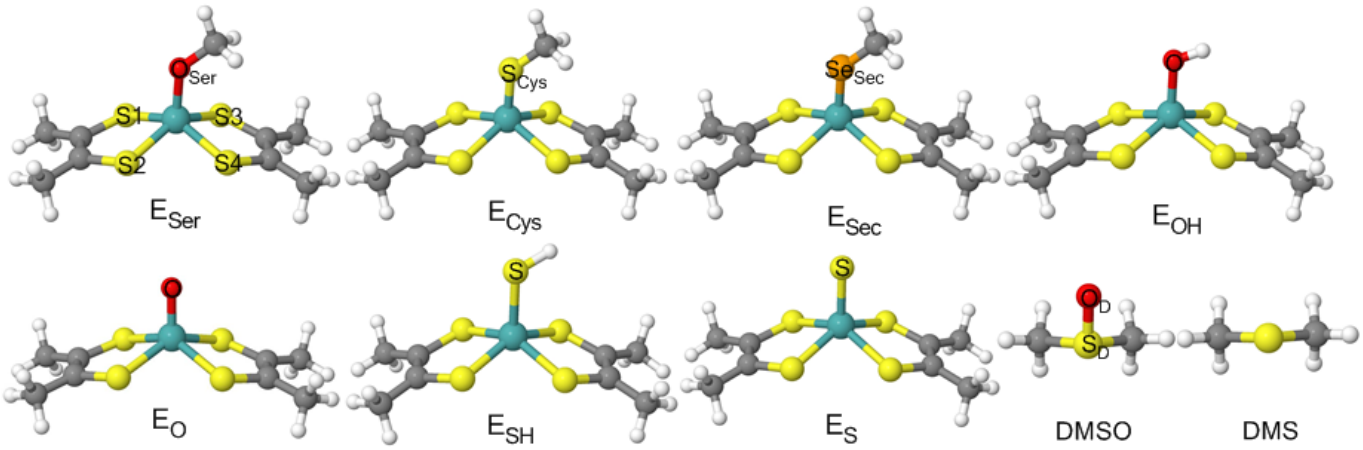

Figure 1. The models of enzyme in the reduced state used in this paper. Structures of the substrate DMSO and the product DMS are also shown.

All calculations were performed with the Turbomole 6.5 [34] package. Geometries were optimised in gas phase at the TPSS [35]/def2-SV(P) [36] level without any symmetry constraints. The energies were improved by single-point calculations using B3LYP [37-39] functional combined with def2-TZVPD [40] basis set. DFT-D3 dispersion corrections were applied to all single-point calculations [41]. Solvent effects were considered by COSMO continuum-solvation model with a dielectric constant of 4 to mimic the protein surrounding [42]. All COSMO calculations involved optimised radii of 1.30, 2.00, 1.72, 2.16, 2.20 and 2.00 Å for H, C, O, S, Se, and Mo, respectively [43]. In all calculations, the resolution-of-identity (RI) approximation was used, expanding the Coulombic interactions in an auxiliary basis set [44, 45]. This approach was selected based on our previous studies of this and other Mo enzymes [15, 25, 46]. They have indicated a strong dependence of the absolute reaction and activation energies on the DFT functional. However, for the difference in energies between the various models in Figure 1, this dependence is much smaller. The Mo–O/S bonds were studied with the natural bond orbital (NBO) method [47] implemented in Gaussian 09 [48] at the TPSS/def2-SV(P), TPSS/def2-TZVP [49], and B3LYP/def2-TZVP levels of theory.

Absolute reduction potentials were calculated from the energy difference between the oxidised and reduced states, corrected to the scale of the normal hydrogen electrode by adding 4.28 V [50]. Likewise, absolute acidity constants were calculated from the energy difference between the deprotonated and protonated states, corrected by a factor of –1131.0 kJ/mol, which represents the hydration free energy of a proton, the translational Gibbs free energy of a proton at 300 K and 1 atm pressure, and the change in reference state from 1 atm to 1 M at 300 K [50].

RESULTS AND DISCUSSION

In this paper, we have studied the DMSOR reaction with QM-cluster calculations. Seven models of the protein-derived ligand were employed to investigate the effect of this ligand, viz. CH_3O^-, CH_3S^-, CH_3Se^-,

OH^-, O^{2-}, SH^-, and S^{2-} (shown in Figure 1). We start with an analysis of the structures of the various active-site models without the substrates. Then, we discuss the other structures in the reaction mechanism, i.e. the intermediate (IM) and the product (P), as well as the two transition states (TS1 and TS2). Finally, we discuss the reaction and activation energies of the various models.

Structures

The structure of the active-site model with the CH_3O^- ligand in the reduced Mo(IV) state (E_{Ser} in Figure 1) was very similar to what has been found in previous studies [16, 17, 21, 22, 24, 29, 30]. The four S ligands were in an approximate square plane with the O_{Ser} atom in an axial position relative to this plane. The Mo–S distances were 2.36–2.37 Å, the Mo–O_{Ser} distance was 1.89 Å, and the Mo–O_{Ser}–C angle was 133°.

In Table 1, we show the corresponding distances and angles in structures in which we have replaced the CH_3O^- ligand with CH_3S^-, CH_3Se^-, OH^-, O^{2-}, SH^-, or S^{2-}. The Mo–X bond lengths (where X is the varying atom in the protein-derived ligands, O, S, or Se) follow the ionic radius of the atom: The bond was shortest with X = O in E_O and longest for Se, as can be seen in Figure 2a. Likewise, the Mo–X–C angle was largest for O and smallest for Se. For the three models with X = S, significant differences can be seen: The Mo–S bond was longest for the SH^- ligand and shortest for the S^{2-} ligand, reflecting the double bond to the metal of the latter. The corresponding trend was also found in the three models with X = O. The Mo–S_{DMDT} bonds were similar in all models (2.35–2.37 Å), except in those with the O^{2-} and S^{2-} ligands, for which they were 2.44 and 2.41 Å, respectively.

Table 1. Structural information for the various active-site models in the reduced RS state (bond lengths in Å and angles in º).

	Mo–X[a]	Mo–X–C	Mo–S1	Mo–S2	Mo–S3	Mo–S4
E_{Ser}	1.89	132.7	2.37	2.37	2.36	2.36
E_{Cys}	2.34	105.1	2.36	2.36	2.35	2.35
E_{Sec}	2.46	101.9	2.36	2.36	2.35	2.35
E_{OH}	1.91	–	2.37	2.37	2.36	2.36
E_O	1.73	–	2.44	2.44	2.44	2.44
E_{SH}	2.37	–	2.36	2.35	2.35	2.35
E_S	2.19	–	2.41	2.41	2.41	2.41

[a] X is the coordinating atom of varying Mo ligand; it is O in E_{Ser}, E_{OH}, and E_O, Se in E_{Sec}, and S in other three models.

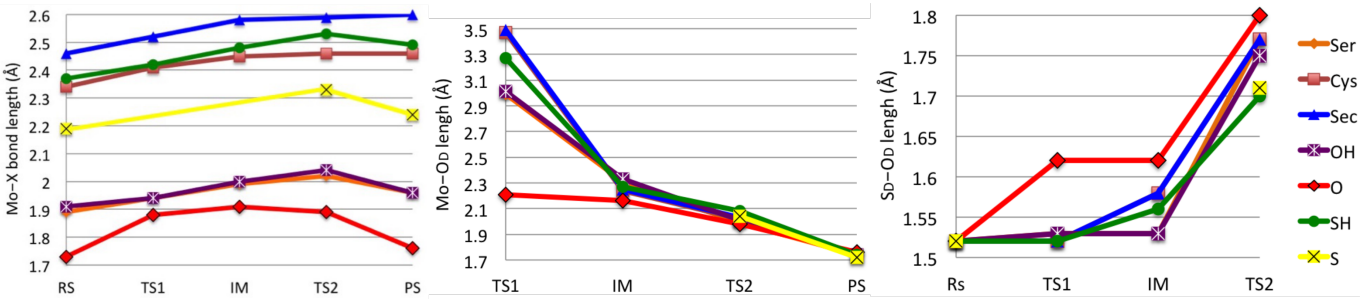

Figure 2. Variation of selected bond length distances in the various states during the reaction with the seven enzyme models: a) Mo–S, b) Mo–O_D and c) S_D–O_D.

Next, we studied the mechanisms of DMSO reacting with the seven enzyme models. For the E_{Ser} model, structures very similar to those found in previous studies were obtained [16, 17, 21, 22, 24, 29, 30]. When DMSO approaches the Mo ion, a transition state (TS1) and an intermediate (IM) were located, as is shown in Figure 3. Key bond distances are collected in Table 2. In IM, the Mo–O_{Ser} bond distance is 0.15 Å longer than in the starting (RS) model (Figure 2a). This is a result of the increase of the

coordination number from five to six when DMSO binds by a Mo–O_D distance of 2.13 Å. The Mo–S_{DMDT} distances are similar to those in the RS state, although they show a larger variation (2.35–2.39 Å).

TS1 is an early (substrate-like) transition state, with a Mo–O_D distance of 2.99 Å (Figure 2b). Consequently, the S_D–O_D bond length is only 0.01 Å longer than for free DMSO (1.52 Å, cf. Figure 2c). It remains the same in IM but increases to 1.77 Å in the second transition state (TS2), in which this bond is being cleaved. Simultaneously, the Mo–O_D bond is shortened by 0.32 Å, reflecting the formation of the Mo=O double bound and the oxidation of Mo from +IV to the +VI state. In the product state (PS), in which the DMS product has dissociated, the Mo–S3 bond (trans to Mo=O) is appreciably longer than the other Mo–S_{DMDT} distances (2.62 Å, compared to 2.44–2.47 Å). The geometry has also changed from prismatic to octahedral, as has been much discussed before [16-27].

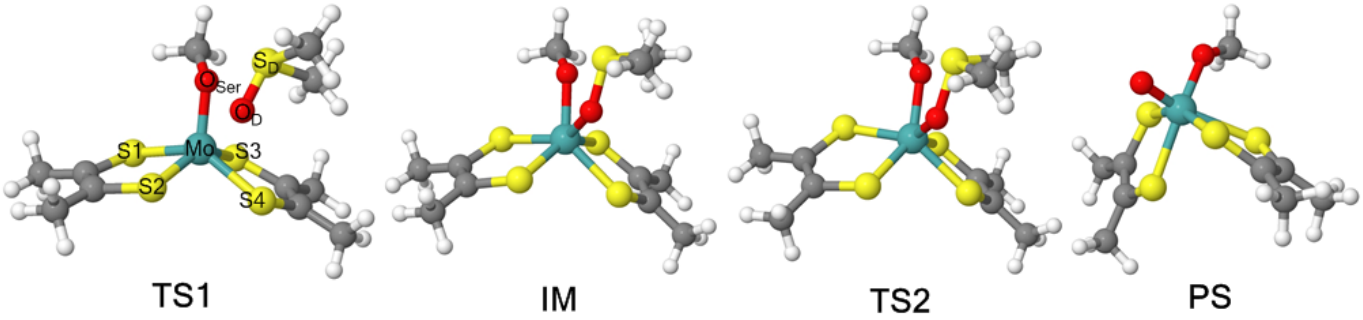

Figure 3. Structures of the various states in the reaction of E_{Ser} with DMSO.

Table 2. Key bond lengths (in Å) for all states in the reaction mechanisms of the five active-site models.

		Mo–X	Mo–S1	Mo–S2	Mo–S3	Mo–S4	Mo–O_D	S_D–O_D	X–S_D
E_{Ser}	TS1	1.94	2.35	2.37	2.37	2.39	2.99	1.53	2.69
	IM	1.99	2.37	2.38	2.37	2.39	2.31	1.53	2.60
	TS2	2.02	2.41	2.42	2.42	2.43	1.99	1.77	2.36
	PS	1.96	2.44	2.47	2.62	2.45	1.74	–	–
E_{Cys}	TS1	2.41	2.35	2.35	2.36	2.37	3.47	1.52	3.22
	IM	2.45	2.38	2.38	2.38	2.42	2.24	1.58	2.98
	TS2	2.46	2.40	2.39	2.41	2.45	2.02	1.77	2.91
	PS	2.46	2.44	2.45	2.59	2.45	1.74	–	–
E_{Sec}	TS1	2.52	2.35	2.35	2.36	2.38	3.49	1.52	4.03
	IM	2.58	2.37	2.37	2.38	2.42	2.25	1.58	3.12
	TS2	2.59	2.40	2.39	2.41	2.45	2.03	1.77	3.03
	PS	2.60	2.44	2.44	2.58	2.44	1.74	–	–
E_{OH}	TS1	1.94	2.34	2.37	2.38	2.40	3.01	1.53	3.49
	IM	2.00	2.35	2.35	2.37	2.40	2.33	1.53	3.13
	TS2	2.04	2.41	2.41	2.42	2.43	2.01	1.75	2.37
	PS	1.96	2.44	2.47	2.62	2.45	1.74	–	–
E_O	TS1	1.88	2.44	2.46	2.43	2.42	2.21	1.62	2.03
	IM	1.91	2.46	2.46	2.45	2.45	2.16	1.62	1.94
	TS2	1.89	2.49	2.48	2.48	2.48	1.98	1.80	1.97
	PS	1.76	2.50	2.67	2.66	2.50	1.76	–	–
E_{SH}	TS1	2.42	2.35	2.35	2.36	2.38	3.27	1.52	3.92
	IM	2.48	2.37	2.37	2.38	2.42	2.27	1.56	3.42
	TS2	2.53	2.39	2.39	2.39	2.42	2.08	1.70	2.86
	PS	2.49	2.45	2.44	2.57	2.45	1.74	–	–
E_S	TS2	2.33	2.47	2.47	2.47	2.47	2.04	1.71	2.53
	PS	2.24	2.46	2.58	2.67	2.46	1.72	–	–

For the E_{Cys}, E_{Sec}, E_{OH}, and E_{SH} models, we obtained the same DMSO reaction mechanism as with the E_{Ser} model. For the E_{Cys} model, the Mo–O_D bond in TS1 was 0.48 Å longer than in the E_{Ser} reaction (Figure 2b), i.e. the interaction between the Mo ion and DMSO was even weaker. Consequently, the S_D–O_D bond length was the same as in free DMSO. The Mo–O_D bond was 0.07 Å shorter in IM than for the E_{Ser} model. The Mo–S_{Cys} bond length was 0.07 Å longer in TS1 than in RS and it was further elongated in the IM, TS2 and PS states. On the other hand, all the Mo–S_{DMDT} distances were similar to those found for E_{Ser} (within 0.03 Å). Likewise, both the S_D–O_D distance in TS2 and the Mo=O_D distance in PS were identical in the two models, showing that the second part of the reaction is little affected by the protein-derived ligand. Comparing the E_{SH} and E_{Cys} models, the Mo–O_D bond in E_{SH} was 0.2 Å shorter in TS1 and 0.06 Å longer in TS2, whereas the S_D–O_D distance in TS2 was 0.07 Å shorter. However, the other bond lengths were similar.

Likewise, there were some small differences between the E_{OH} and E_{Ser} models: The Mo–O bonds in IM and TS2 were 0.01–0.03 Å longer for the E_{OH} model, the Mo–O_D bond was 0.02 Å longer in TS1, IM and TS2, and the S_D–O_D bond was 0.02 Å shorter in TS2. For the E_{Sec} model, all bond distances were similar to those obtained with the E_{Cys} model (within 0.01 Å), besides the Mo–Se bond that was 0.11–0.14 Å longer than Mo–S bond. In particular, the Mo–O_D bond in TS1 was still very long (3.49 Å) and the S_D–O_D distance in TS2 was identical to that of the E_{Ser} model.

For the E_O model, a two-step reaction mechanism was also found. However, it was rather different from that of the five singly charged varying models. In particular, the intermediate IM was more symmetric with a short interaction between O and S_D (1.94 Å; the O_D–S_D bond is 1.62 Å) and therefore a long Mo–O bond, 1.91 Å (1.73 Å in RS; cf. Figure 4a). The other models also have rather short X–S_D interactions, in particular in TS2 (2.36–3.03 Å), indicating that the latter is stabilised by this interaction. However, in IM, the X–S_D distance is much larger than for E_O, e.g. 3.13 Å for E_{OH}. TS1 was very late and similar to IM (for example, the Mo–O_D bond is 2.21 Å in TS1 and 2.16 Å in IM). TS2 was even more symmetric with Mo–O distances of 1.89 and 1.98 Å, and S_D–O distances of 1.96 and 1.80 Å (Figure 4b).

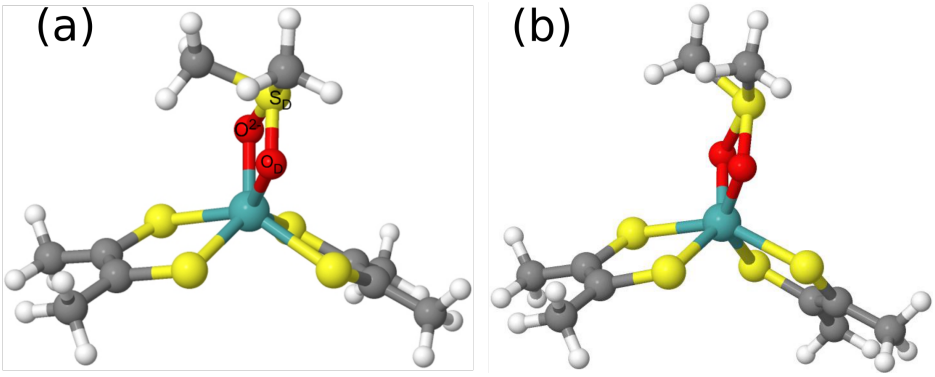

Figure 4. Structures of the IM (a) and TS2 (b) states with the E_O model.

In sharp contrast, the reaction mechanism of the E_S model was found to be different. In particular, no intermediate could be found. Instead, the O_D atom was transferred directly to the Mo ion, through a transition state that is analogous to TS2 for the other models. For example, the Mo–O_D and S_D–O_D bonds were 2.04 and 1.71 Å, which are close to what was found for TS2 for the other models, in particular the E_{SH} model.

Energies of the DMSOR reaction

Next, we discuss the reaction energies for the seven models with the various protein-derived ligands. All the energies are based on single-point calculations with the B3LYP-D3 functional and the def2-TZVPD basis set in a COSMO continuum solvent. The energies can be used to understand the effect of the varying ligand. The first step, DMSO binding, was endothermic by 24, 29, 27, 25, and 20 kJ/mol in the E_{Ser}, E_{Cys}, E_{Sec}, E_{OH}, and E_{SH} models, respectively, as can be seen in Figure 5. The activation barrier for this step was 34, 34, 25, 29, and 27 kJ/mol. The energy barrier for the second step was 61, 52, 55, 41, and

50 kJ/mol. Thus, for the three models with protein-derived ligands and the model with OH^-, the activation energy for the complete reaction was nearly identical, 81–85 kJ/mol, whereas it was slightly smaller with the SH^- ligand, 69 kJ/mol. The full reaction was exothermic by 56, 69, 74, 52, and 69 kJ/mol (relative to RS), respectively, showing that E_{OH} gave the least exothermic reaction and E_{Sec} the most exothermic reaction, and SH^- gave the same reaction energy as CH_3S^-. These trends are similar to those found in a comparison of the intrinsic reactivity of the three mononuclear Mo enzyme families [26].

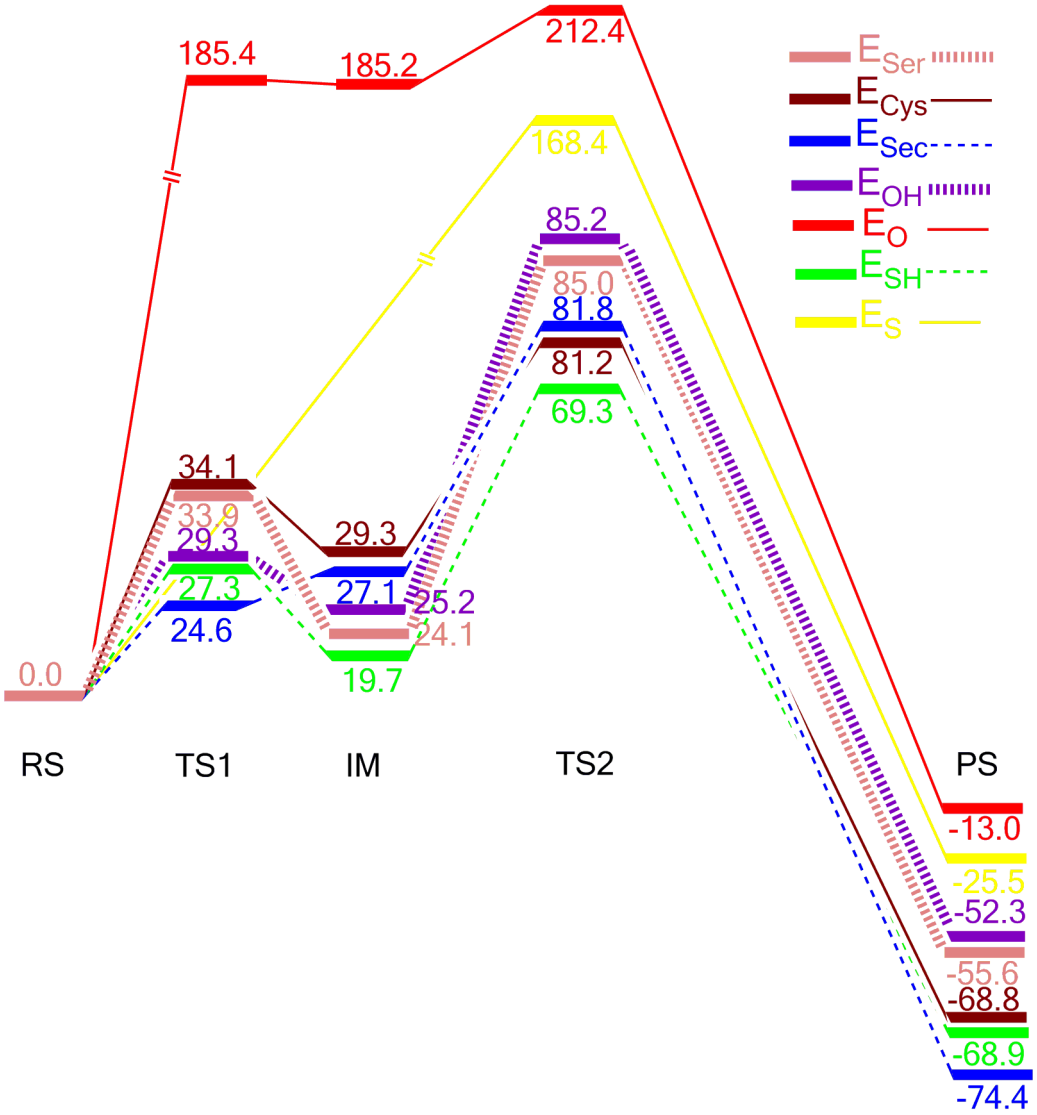

Figure 5. The reaction energy profiles (in kJ/mol relative to RS) in the various models obtained at the B3LYP/def2-TZVPD level of theory in a COSMO continuum solvent. Note that the energy levels are not in scale to emphasize the difference among the different models for the various states.

In contrast, the activation energies for the E_O and E_S models were very high, 212 and 168 kJ/mol, respectively, twice as high as for the other protein models. Apparently, the extra negative charge of the $O^{2-}$and S^{2-} models increases the activation barrier by 87–127 kJ/mol, partly by destabilising the product state by 39–43 kJ/mol.

Several attempts were made to explain the large activation barrier in these two models. We have seen above that the structures of IM and TS2 of the E_O model are quite different from those of the other models (compare Figures 3 and 4). The Mo–O_D bond distance in TS2 was 1.98 Å, which is slightly shorter than that in the E_{Ser} (1.99 Å) and E_{OH} (2.01 Å) models. Moreover, the S_D–O_D bond in TS2 was 0.03 and 0.05 Å longer than in the E_{Ser} and E_{OH} models. This indicates that TS2 in E_O is slightly later than in the E_{Ser} and E_{OH} models. All the Mo–S_{DMDT} bonds were longer in E_O. In addition, the Mo–O bonds in

RS and TS2 were 0.18 and 0.15 Å shorter in E_O than in E_{OH}, which is caused by the negative change of O^{2-} group. The results in Table 3 shows that the Mo–O bond of RS in the E_O model is very strong with a Wiberg bond index of 2.01, reflecting a Mo=O double bond. However, the bond index decreases to 1.36 in TS2, which is also reflected by a much longer Mo–O bond (cf. Figure 2a). This decrease is larger than in E_{OH} model, for which the Wiberg bond index changes from 1.34 to 0.93. This indicates that high barrier in the E_O model may be partly caused by the need of weakening the Mo–O bond.

For the X = S models, we compared the O_D–S_D bond distances of TS2, which were 1.77, 1.70, and 1.71 Å in E_{Cys}, E_{SH}, and E_S, respectively, showing that the distance in the E_S model is similar to that in the E_{SH} model. Likewise, no dramatic difference was found in the Mo–O_D bond length in TS2: It was 2.04 Å in the E_S model, which is between that in E_{Cys} (1.99 Å) and in E_{SH} (2.08 Å). Increasing the dielectric constant of the COSMO model further increased the activation energy of the E_S model, e.g. to 188 kJ/mol with a dielectric constant of 80.

The Mo–S bond length was 2.34, 2.46, and 2.46 Å in the RS, TS2, and PS states, respectively, for the E_{Cys} model. It can be seen in Figure 2a that it was 0.03–0.06 Å longer in E_{SH} model. However, in the E_S model, the Mo–S bond was appreciably shorter because the negative charge of S^{2-}, 2.19, 2.33, and 2.24 Å, respectively. If we look at the doubly occupied 3*p* orbitals of the S^{2-} in the RS and TS2 states (Figure 6), some interactions between the S^{2-} 3*p* and Mo 4*d* orbitals are different. In the RS state, it can be seen that the S^{2-} 3*p* orbitals interact with the Mo $4d_{z2}$, $4d_{xz}$, and $4d_{yz}$ orbitals. However, in the TS2 state, the interactions of the S^{2-} orbitals with the Mo $4d_{xz}$, and $4d_{yz}$ orbitals are less clear. This is supported by the Wiberg bond index of the Mo–S bond, which show that the bond order decreases from 2.22 to 1.56 when going from RS to TS2 (Table 3). This leads to an elongation of the Mo–S bond by 0.14 Å. On the other hand, in the E_{Cys} and E_{SH} models, the Mo–S bond distances are more than 2.34 Å, which is 0.01 Å longer than in TS2 of E_S model. This reflects that the S 3*p* and Mo 4*d* interactions in the RS state are weaker, as shown in Figure 6. Again, this is supported by the Wiberg bond index, which shows that the Mo–S bond order is only 1.48 in RS. It further decreases to 1.02 in TS, but this decrease is smaller in the E_{SH} model than in the E_S model. Thus, the destabilisation is smaller in E_{SH} than in E_S, which may explain its lower activation energy.

Table 3. Wiberg bond indices of the Mo–X bond in the RS and TS2 states of the E_O, E_{OH}, E_S, and E_{SH} models, calculated at the B3LYP/def2-TZVP level of theory.

Model	bond index	
	RS	TS2
E_O	2.01	1.36
E_{OH}	1.34	0.93
E_S	2.22	1.56
E_{SH}	1.48	1.02

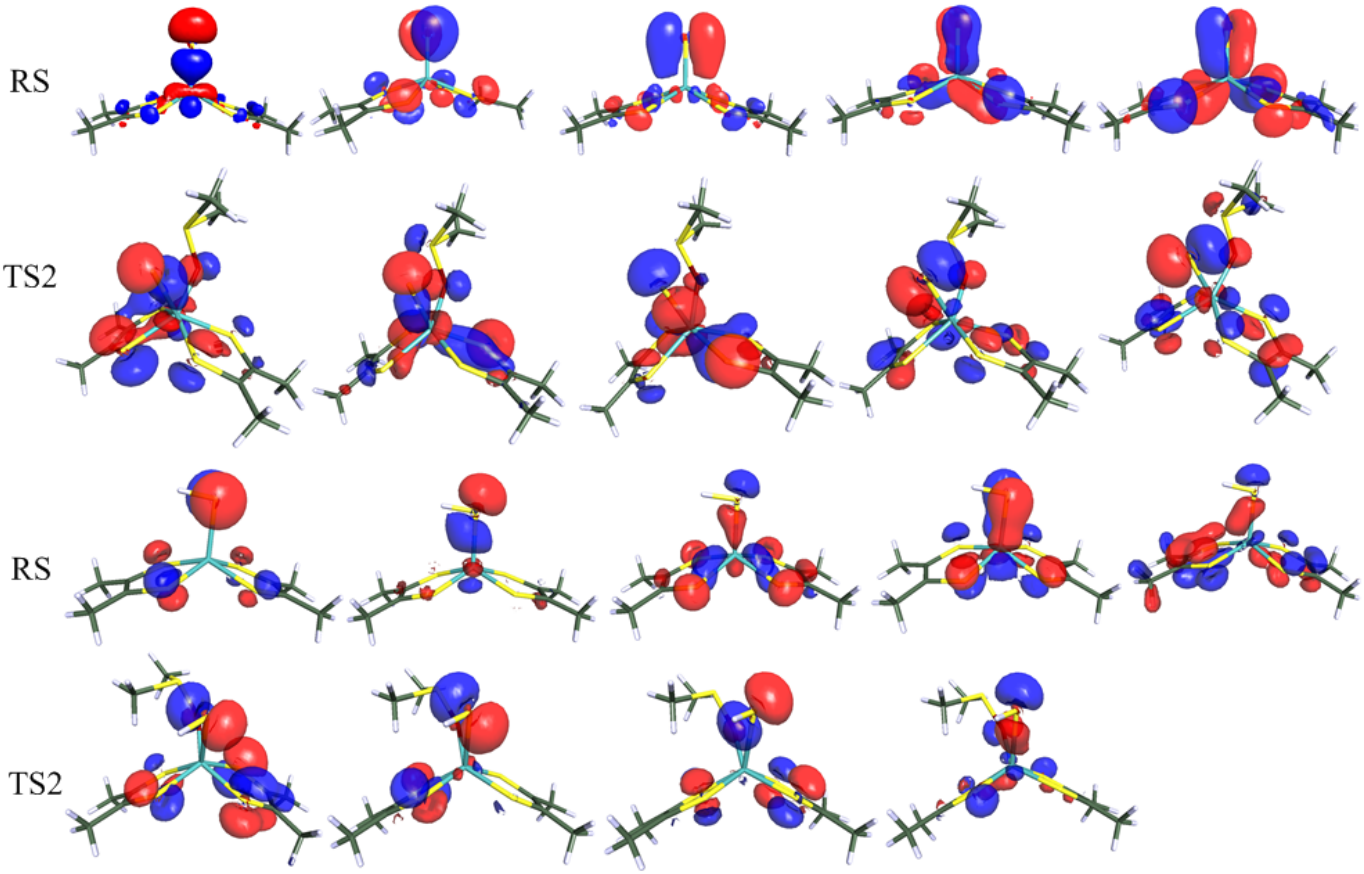

Figure 6. Molecular orbitals with large contributions of the S^{2-} ligand in the E_S (the two rows on the top) and E_{SH} models (the lower two rows), obtained at the TPSS/def2-SV(P) level of theory.

Reduction potential and water binding energy

Finally, we compared two additional sets of reaction energies of the various DMSOR models. After the dissociation of the DMS product, the oxidised active site needs to be reduced back to the Mo(IV) state, before it can react with DMSO again. This is supposed to take place by two coupled electron- and proton-transfer step, using electrons from an external source, i.e. involving $Mo^{V}OH$ and $Mo^{IV}H_2O$ intermediates [1, 5-7]. From the latter intermediate, the RS state is recovered by dissociation of the water molecule. By optimising models of these two intermediates, we can investigate also how the protein-derived ligand affects also the re-reduction of the active site [26].

First, we calculated the energy of the coupled electron- and proton-transfer steps. The results in Table 4 show that the five models with a single negative charge gave similar reduction potentials for both reactions, 0.19–0.26 V for the first transfer and 0.06–0.25 V for the second transfer. In both cases, the reduction potentials were positive, indicating that active sites have been designed for a facile re-reduction of the active sites, in accordance with our previous comparison of the three OAT Mo enzyme families [26]. On the other hand, the E_O and E_S models gave more differing results: The potential was 0.87–1.06 V for the second coupled electron–proton transfer V, i.e. 0.6–1.0 V more positive than for the other five models, whereas it was more similar for the first transfer 0.17 or –0.15 V. This is mainly an effect of the extra negative charge of the model.

Table 4. Energies for the coupled electron and proton transfer going from the $Mo^{VI}O(DMDT)_2(X)$ state, via $Mo^{V}(OH)(DMDT)_2(X)$ ($\Delta G_{6\rightarrow5}$), to the $Mo^{VI}(OH_2)(DMDT)_2(X)$ state ($\Delta G_{5\rightarrow4}$), with X = CH_3O^-, CH_3S^-, CH_3Se^-, OH^-, O^{2-}, SH^-, or S^{2-} (for O^{2-} and S^{2-} a $Mo^{VI}(DMDT)_2(X)$ state was used instead, because the water molecule dissociated in the reduced state). The energies were calculated at the B3LYP+D3/def2-TZVPD level of theory in a COSMO continuum solvent with a dielectric constant of 4 and they expressed as redox potentials in V.

Reaction	E_{Ser}	E_{Cys}	E_{Sec}	E_{OH}	E_O	E_{SH}	E_S
$\Delta G_{6\rightarrow5}$	0.19	0.23	0.20	0.24	0.17	0.26	-0.15
$\Delta G_{5\rightarrow4}$	0.25	0.18	0.15	0.23	0.87	0.06	1.06

Finally, we also calculated the binding energy of a water molecule to the RS complex. Again, the energies of the E_{Ser}, E_{Cys}, E_{Sec}, and E_{SH} models gave similar results, 5–16 kJ/mol, indicating that the binding of water is unfavourable, i.e. that the Mo(IV)(OH_2) intermediate spontaneously is expected to dissociate the water ligand, forming the RS state, ready to bind the DMSO substrate. On the other hand, for the E_O and E_S models, no stable structure for a six-coordinate model with water coordinated to Mo(IV) could be found. Instead, the water molecule preferred to bind in the second coordination sphere. Therefore, no water-binding energies are given for these models in Table 5.

Table 5. Binding energies (ΔG_{bind} in kJ/mol) of a water molecule to the RS complex, i.e. the energy of $Mo^{VI}(DMDT)_2(X) + H_2O \rightarrow Mo^{VI}(DMDT)_2(X)(OH_2)$ reaction, with X = CH_3O^-, CH_3S^-, CH_3Se^-, OH^-, or SH^-. The energies were calculated at the B3LYP+D3/def2-TZVPD level of theory in a COSMO continuum solvent with a dielectric constant of 4.

	ΔG_{bind}
E_{Ser}	16.4
E_{Cys}	5.4
E_{Sec}	6.0
E_{OH}	16.3
E_{SH}	13.6

CONCLUSIONS

In this paper, we have studied how the DMSOR reaction mechanism is modified when the protein-derived ligand is varied. With Ser, Cys, SeCys, OH^-, and SH^- models, the same mechanism was obtained, in which the substrate first binds to Mo, and then the S_D–O_D bond is cleaved to generate the product. All five models gave similar activation barriers of 69–85 kJ/mol. However, with O^{2-} and S^{2-} models, the activation barriers were much higher, 212 and 168 kJ/mol. The E_O model gave also a two-step reaction with a nearly symmetric TS2, whereas the E_S model gave a one-step reaction without any intermediate. The high activation energies with O^{2-} and S^{2-} ligands are probably caused by less exothermic reaction energies (13–25 compared to 52–74 kJ/mol) and a stronger stabilisation of the reactant state by the strong (double) Mo–S^{2-} or Mo–O^{2-} bonds. These results indicate that it is likely that the oxo and sulfido ligands are protonated (to OH^- or SH^-) during the reaction of enzymes employing these ligands, e.g. in arsenate oxidase [1, 7, 9, 33].

Acknowledgements

This investigation has been supported by grants from the Swedish research council (project 2014-5540), from the China Scholarship Council, and from COST through Action CM1305 (ECOSTBio). The computations were performed on computer resources provided by the Swedish National Infrastructure for Computing (SNIC) at Lunarc at Lund University. We acknowledge fruitful discussions with Prof. Silke Leimkühler, Potsdam.

References

[1] R. Hille Chem. Rev. 96 (1996) 2757-2816
[2] R. Hille Met. Ions Biol. Syst. 39 (2002) 187-226
[3] Y. Zhang, V.N. Gladyshev J. Mol. Biol. 379 (2008) 881-899
[4] R. Hille Trends Biochem. Sci 27 (2002) 360-367
[5] M.J. Romao, J. Knablein, R. Huber, J.J.G. Moura Prog. Biophys. Mol. Bio. 68 (1997) 121-144
[6] A. Rajapakshe, A.V. Astashkin, E.L. Klein, D. Reichmann, R.R. Mendel, F. Bittner, J.H. Enemark Biochemistry 50 (2011) 8813-8822
[7] R. Hille, J. Hall, P. Basu Chem. Rev. 114 (2014) 3963-4038
[8] A.S. McAlpine, A.G. McEwan, S. Bailey J. Mol. Biol. 275 (1998) 613-623
[9] P.J. Ellis, T. Conrads, R. Hille, P. Kuhn Structure 9 (2001) 125-132
[10] B.S. Lim, K.M. Sung, R.H. Holm J. Am. Chem. Soc. 122 (2000) 7410-7411
[11] P.D. Smith, A.J. Millar, C.G. Young, A. Ghosh, P. Basu J. Am. Chem. Soc. 122 (2000) 9298-9299
[12] K.M. Sung, R.H. Holm J. Am. Chem. Soc. 123 (2001) 1931-1943
[13] R. Hille Arch. Biochem. Biophys. 433 (2005) 107-116
[14] G. Schwarz, R.R. Mendel Annu. Rev. Plant. Biol. 57 (2006) 623-647
[15] R.H. Holm, E.I. Solomon, A. Majumdar, A. Tenderholt Coord. Chem. Rev. 255 (2011) 993-1015
[16] A.L. Tenderholt, J.J. Wang, R.K. Szilagyi, R.H. Holm, K.O. Hodgson, B. Hedman, E.I. Solomon J. Am. Chem. Soc. 132 (2010) 8359-8371
[17] J.L. Li, R.A. Mata, U. Ryde J. Chem. Theor. Comput. 9 (2013) 1799-1807
[18] A. Thapper, R.J. Deeth, E. Nordlander Inorg. Chem. 38 (1999) 1015-1018
[19] C.E. Webster, M.B. Hall J. Am. Chem. Soc. 123 (2001) 5820-5821
[20] A. Thapper, R.J. Deeth, E. Nordlander Inorg. Chem. 41 (2002) 6695-6702
[21] J.P. McNamara, J.A. Joule, I.H. Hillier, C.D. Garner Chem. Commun. (2005) 177-179
[22] J.P. McNamara, I.H. Hillier, T.S. Bhachu, C.D. Garner Dalton Trans. (2005) 3572-3579
[23] M. Hofmann Inorg. Chem. 47 (2008) 5546-5548
[24] E. Hernandez-Marin, T. Ziegler Can. J. Chem. 88 (2010) 683-693
[25] S. Metz, W. Thiel Coord. Chem. Rev. 255 (2011) 1085-1103
[26] J.L. Li, U. Ryde Inorg. Chem. 53 (2014) 11913-11924
[27] J.L. Li, M. Andrejic, R.A. Mata, U. Ryde Eur. J. Inorg. Chem. (2015) 3580-3589
[28] M. Mohr, J.P. McNamara, H. Wang, S.A. Rajeev, J. Ge, C.A. Morgado, I.H. Hillier Faraday Discuss. 124 (2003) 413-428
[29] M. Hofmann J. Mol. Struc-Theochem 773 (2006) 59-70
[30] A.L. Tenderholt, K.O. Hodgson, B. Hedman, R.H. Holm, E.I. Solomon Inorg. Chem. 51 (2012) 3436-3442
[31] R.L. McNaughton, B.S. Lim, S.Z. Knottenbelt, R.H. Holm, M.L. Kirk J. Am. Chem. Soc. 130 (2008) 4628-4636
[32] M.R.A. Blomberg, T. Borowski, F. Himo, R.Z. Liao, P.E.M. Siegbahn Chem. Rev. 114 (2014) 3601-3658
[33] T.P. Warelow, M. Oke, B. Schoepp-Cothenet, J.U. Dahl, N. Bruselat, G.N. Sivalingam, S. Leimkuhler, K. Thalassinos, U. Kappler, J.H. Naismith, J.M. Santini Plos One 8 (2013)
[34] TURBOMOLE V6.5 2013, a development of University of Karlsruhe and Forschungszentrum Karlsruhe GmbH, 1989–2007, TURBOMOLE GmbH, since 2007; available from http://www.turbomole.com.
[35] J. Tao, J.P. Perdew, V.N. Staroverov, G.E. Scuseria Phys. Rev. Lett. 91 (2003) 146401
[36] A. Schäfer, H. Horn, R. Ahlrichs J. Chem. Phys. 97 (1992) 2571-2577
[37] A.D. Becke Phys. Rev. A 38 (1988) 3098-3100
[38] C.T. Lee, W.T. Yang, R.G. Parr Phys. Rev. B 37 (1988) 785-789
[39] A.D. Becke J. Chem. Phys. 98 (1993) 5648-5652
[40] D. Rappoport, F. Furche J. Chem. Phys. 133 (2010)
[41] dftd3 software http://www.thch.uni-bonn.de/tc/index.php?section=downloads&subsection=DFT-D3&lang=english
[42] A. Klamt, G. Schuurmann J. Chem. Soc., Perkin Trans. 2 (1993) 799-805

[43] A. Klamt, V. Jonas, T. Burger, J.C.W. Lohrenz J. Phys. Chem. A 102 (1998) 5074-5085
[44] K. Eichkorn, O. Treutler, H. Öhm, M. Häser, R. Ahlrichs Chem. Phys. Lett. 240 (1995) 283-290
[45] K. Eichkorn, F. Weigend, O. Treutler, R. Ahlrichs Theor. Chem. Acc. 97 (1997) 119-124
[46] M.C. van Severen, M. Andrejic, J.L. Li, K. Starke, R.A. Mata, E. Nordlander, U. Ryde J. Biol. Inorg. Chem. 19 (2014) 1165-1179
[47] T.K. Brunck, F. Weinhold J. Am. Chem. Soc. 101 (1979) 1700-1709
[48] M. J. Frisch, G. W. Trucks, H. B. Schlegel, G. E. Scuseria, M. A. Robb, J. R. Cheeseman, G. Scalmani, V. Barone, B. Mennucci, G. A. Petersson, H. Nakatsuji, M. Caricato, X. Li, H. P. Hratchian, A. F. Izmaylov, J. Bloino, G. Zheng, J. L. Sonnenberg, M. Hada, M. Ehara, K. Toyota, R. Fukuda, J. Hasegawa, M. Ishida, T. Nakajima, Y. Honda, O. Kitao, H. Nakai, T. Vreven, J. A. Montgomery, Jr., J. E. Peralta, F. Ogliaro, M. Bearpark, J. J. Heyd, E. Brothers, K. N. Kudin, V. N. Staroverov, R. Kobayashi, J. Normand, K. Raghavachari, A. Rendell, J. C. Burant, S. S. Iyengar, J. Tomasi, M. Cossi, N. Rega, J. M. Millam, M. Klene, J. E. Knox, J. B. Cross, V. Bakken, C. Adamo, J. Jaramillo, R. Gomperts, R. E. Stratmann, O. Yazyev, A. J. Austin, R. Cammi, C. Pomelli, J. W. Ochterski, R. L. Martin, K. Morokuma, V. G. Zakrzewski, G. A. Voth, P. Salvador, J. J. Dannenberg, S. Dapprich, A. D. Daniels, Ö. Farkas, J. B. Foresman, J. V. Ortiz, J. Cioslowski, and D. J. Fox, Gaussian, Inc., Wallingford CT, 2009.
[49] F. Weigend, R. Ahlrichs Phys. Chem. Chem. Phys. 7 (2005) 3297-3305
[50] C.P. Kelly, C.J. Cramer, D.G. Truhlar J. Phys. Chem. B 110 (2006) 16066-16081

Graphical abstract and synopsis

The effect of varying the protein-derived ligand in dimethyl sulfoxide reductase (serine, cysteine, selenocysteine, OH^-, O^{2-}, SH^-, or S^{2-}) has been studied by density-functional theory. The five ligands with a single negative charge give similar results, whereas O^{2-} and S^{2-} give differing mechanisms and much higher barriers.

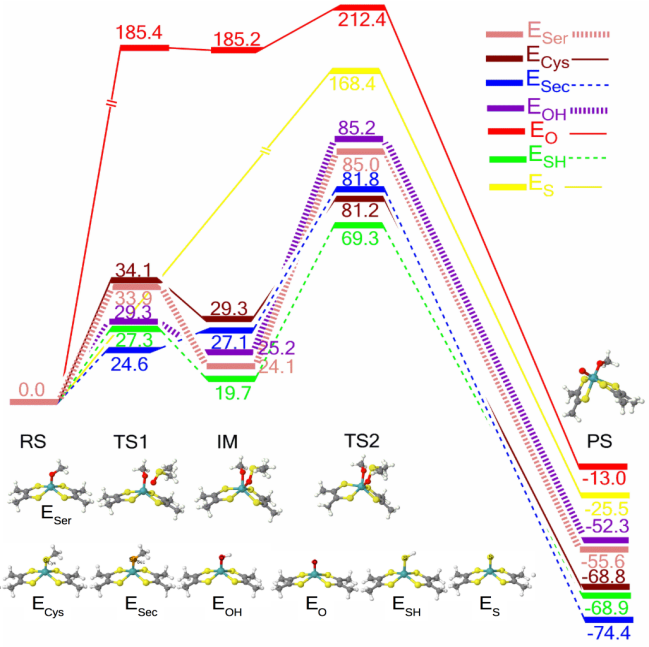

Highlights

- Serine, cysteine, selenocysteine, OH^- and SH^- give a two-step mechanism
- The substrate first binds to Mo and then the O–S bond is cleaved and Mo is oxidised
- The activation barriers are 69–85 kJ/mol and the reaction energies are 52–74 kJ/mol
- O^{2-} and S^{2-} give higher activation barriers (168–212 kJ/mol) and differing mechanisms
- Caused by less exothermic reaction energies and the strong Mo–O^{2-} or Mo–S^{2-} bonds